3.8 Imaging the sea surface imprints of Atmospheric Vortex Streets by space-borne Synthetic Aperture Radar

Xiaofeng Li[1], P. Clemente-Colón[1], W. Pichel[1], P. Vachon[2], and K. Friedman[1]

[1]NOAA E/RA3, WWBG, Room 102, 5200 Auth Road, Camp Springs, MD 20746, U.S.A.
Email: Xiaofeng.Li@noaa.gov

[2]Canada Centre for Remote Sensing, 588 Booth St., Ottawa, Ontario K1A 0Y7, Canada

1. INTRODUCTION

Remote sensing images are often used to study meso-scale atmosphere phenomena in the marine atmosphere boundary layer (MABL) over large ocean areas. These phenomena, cause fluctuations in atmospheric wind speed, temperature and moisture content. On one hand, at the top of MABL, these fluctuations modulate the moisture pattern so that they cause signatures in the cloud patterns, which can be imaged by visible and infrared satellite sensors. On the other hand, these fluctuations modulate the sea surface roughness. A synthetic aperture radar (SAR) senses the ocean surface roughness through a Bragg scattering mechanism. Therefore, SAR can observe any atmospheric process that modulates near surface wind field. Such examples include atmospheric lee waves (Vachon *et al.*, 1994; Li, *et al.* 1998, Zheng *et al.*, 1998), gravity waves (Thomson *et al*., 1992; Chunchuzov *et al.*, 2000), atmospheric boundary layer rolls (Alpers and Brümmer, 1994; Mourad, 1996; Pichel *et al*. 2000), atmospheric fronts (Mourad, 1999), mesoscale phenomena such as polar mesoscale cyclones and hurricanes (Friedman and Li, 2000), and more recently atmospheric vortex streets (Li *et al*. 2000).

In this study, the sea surface imprint of atmospheric vortex streets (AVS) observed on two RADARSAT Synthetic Aperture Radar (SAR) images of the Aleutian Islands in the western Gulf of Alaska during NOAA's Alaska SAR demonstration period (1999-2001) are analyzed. The AVS's are interpreted as the atmosphere analog of classic Von Karman vortex streets. The AVS length is typical over 200 km, and there are several pairs of vortices within the AVS. Although atmospheric vortex shedding from large islands was suggested as early as the 1930's, it was not until the early 1960's that researchers observed the AVS pattern in the atmosphere in cloud images taken by the first generation of earth orbiting satellites. AVS's were not observed prior to the advent of satellites due to the AVS scale of 100 to 400 km; too small to be delineated by a synoptic observation network and too large to be observed by a single station.

In this study, we analyze the first few cases of AVS observed by SAR. Using SAR image, we can measure the basic properties of AVS, i.e., the ratio of vortex spacing (a) and the width of the Von Kármán vortex street (h). We found that the *a/h* ranges between 0.35 and 0.45.

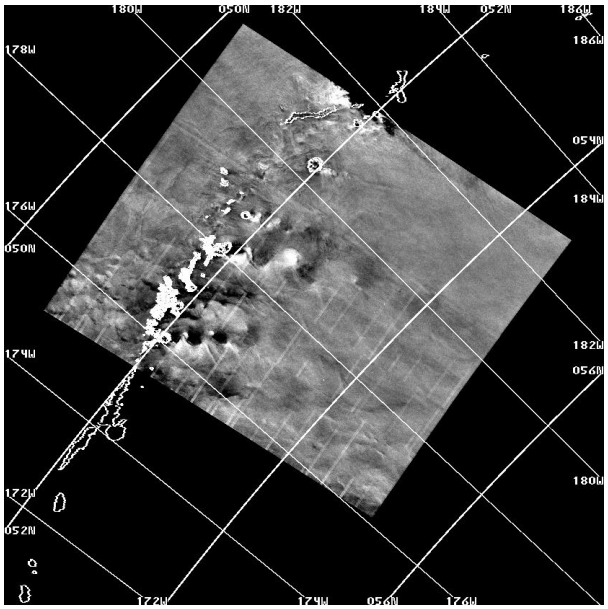

Fig. 1 A RADARSAT ScanSAR wide B SAR subimage containing the sea surface imprint of four AVS's. The image center is at N52° and W178°, and was acquired at 05:40:04 UTC on May 12, 2000. (© Canadian Space Agency, 2000).

On the basis of these SAR images, surface pressure maps and nearby radiosonde station observations, the vortex shedding period, the tangential velocity at the outer edge of the vortex, the vortex lifetime at the SAR acquisition time, and the total energy dissipation are estimated using

the Von Kármán vortex streets theory. We also calculate the range of Reynolds number, the Strouhal number (S), the Lin number and kinematic viscosity number, which can support the AVS shedding.

2. DATA

The RADARSAT SAR images (Figuew 1 and 2) considered in this study are ScanSAR Wide B scenes that were processed at the Alaska SAR Facility as a QuickLook product (i.e., to a spatial resolution of 200 m with a pixel spacing of 100 m). All the SAR images are acquired in Aleutian Islands in the Gulf of Alaska.

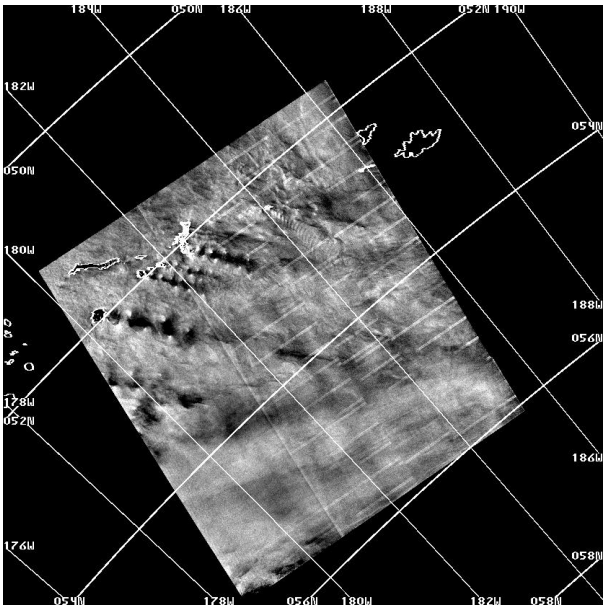

Fig. 2. A RADARSAT ScanSAR wide B SAR subimage containing the sea surface imprint of four AVS's. The image center is at N54^o and E2^o, and was acquired at 18:27:35 UTC on March 22, 2001. (© Canadian Space Agency, 2001).

3. ATMOSPHERIC VORTEX STREET

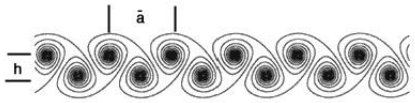

Fig. 3. Schematic plot of a Kármán vortex street generated by wind passing a cylindrical obstacle of diameter D. a is the vortex spacing, and h is the width of the Kármán vortex street.

The AVS pattern consists of a double row of counter rotating vortex-pairs shedding alternately near each edge of the obstacle and resembles the classic Von Kármán vortex-street patterns (Fig. 3 and 4).

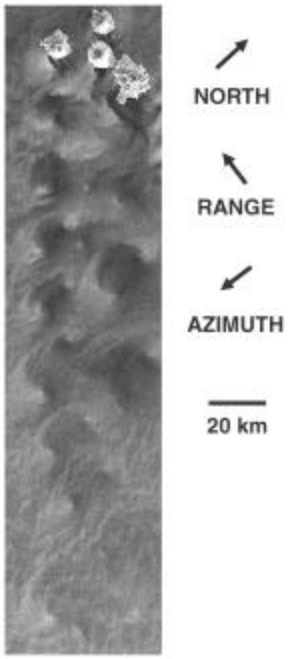

Fig. 4. A RADARSAT ScanSAR wide B SAR subimage containing the sea surface imprint of two AVS's. The image center is at N52^o and W172^o, and covers the western side of the Gulf of Alaska. The image was acquired at 17:25:41 UTC on May 5, 1999. (© Canadian Space Agency, 1999)

The basic properties of the AVS's are the *h/â* ratio, where h is the distance between the two streets and *â* is the wavelength within the same street.

$$f = \frac{Ue}{\bar{a}} = \frac{U_O}{\bar{a}}\left(\frac{U_e}{U_O}\right) \qquad (1)$$

where *f* is the vortex shedding rate or frequency. U_e is the vortex propagation velocity, and U_o is the undisturbed wind velocity. The relation between U_e and U_o is: [Li, *et al*. 2000]:

$$4\pi(h/\bar{a})(U_e/U_O)(1-U_e/U_O)=1 \qquad (2)$$

The rate of viscous dissipation of vortex energy ε is:

$$\varepsilon = (k^2/8\pi^2R^2t)[1-e^{(-R^2/2\nu t)}] \qquad (3)$$

The total energy dissipated by a vortex during its lifetime is:

$$\frac{1}{r_o}\int_{t_o}^{t} e dt = \frac{1}{r_o}(k^2/16p^2 n t_o)[1+\sum_{n=1}^{\infty}\frac{(-R/2ut_o)^n}{(n+1)\cdot(n+1)!}] \qquad (4)$$

From these SAR images, the ration is measured to be about 0.40 to 0.45. The U_o is obtained from nearby radiosounde measurements. Therefore, using above equations, we can estimate that basic properties of the AVS. The AVS shedding period is between 30 to 50 minutes; the total energy dissipation is around 25 J/m^3.

The Reynolds Number, $Re = \frac{U_o d}{\nu}$, is about 200. The Froude number, $F = U/\sqrt{gd}$, is less than 0.2.

4. DISCUSSIONS

From this analysis, we see that if AVS patterns are observed by consecutive remote sensing images, the propagation velocity (*Ue*) and the length (*L*) may be measured from the images, thus allowing direct calculation of the vortex shedding rate (*f*) and lifetime (*t*).

In order to observe the AVS, visible and infrared sensors require high atmosphere moisture content so that clouds associated with the AVS wind pattern can be imaged. The SAR does not have this constraint since it images the sea surface imprint of the AVS. SAR coupled with visible and infrared sensors could provide the top and bottom patterns of the AVS. As the number of SAR sensors increases over the coming years, it is likely that simultaneous imaging (SAR, visible, and infrared) of an AVS will become available for more detailed AVS studies.

References

Alpers, W., and B. Brümmer, Atmospheric boundary layer rolls observed by the synthetic aperture radar aboard the ERS 1 satellite, *J. Geophys. Res., 99,* 12,613-12,621, 1994.

Chunchuzov, I., P. W. Vachon, and X. Li, Analysis and modelling of atmospheric gravity waves observed in RADARSAT SAR images, *Remote Sensing of Environment*, in press, 2000.

Friedman, K. and X. Li, Storm patterns over the ocean with wide swath SAR, *Johns Hopkins University Applied Physics Lab Technical Digest*, 21(1), 80-85, 2000.

Li, X., W. G. Pichel, K. S. Friedman, and P. Clemente-Colón, The sea surface imprint of island lee waves as observed by RADARSAT synthetic aperture radar, *Proceeding of IEEE Geoscience and Remote Sensing Conference*, 763-766. Seattle, Washington, 1998.

Li, Xiaofeng, P. Clemente-Colon, W. G. Pichel and P. W. Vachon, Atmospheric vortex streets on a RADARSAT SAR image, Geophysical Research Letters, Vol. 27, No.11, 1655-1658, 2000.

Mourad, P. D., Footprints of Atmospheric Phenomena in Synthetic Aperture Radar Images of the Ocean Surface- a review. Chapter 11 in "*Air-sea fluxes -physics, chemistry, and dynamics"*, edited by G. Geernaert, *Kluwer Academic Publishers*, Dordrecht, Holland, 640pp., 1999.

Mourad, P. D., Inferring multiscale structures in atmospheric turbulence using satellite-based SAR imagery, *J. Geophys. Res.* 101, 18,433-18449, 1996.

Pichel, W. G. and P. Clemente-Colon, CoastWatch SAR applications and demonstrations, *Johns Hopkins University Applied Physics Lab Technical Digest*, 21(1), 49-57, 2000.

Thomson, R. E., P. W. Vachon, and G. A. Borstad, Airborne synthetic aperture radar imageery of atmospheric gravity waves, *J. Geophys. Res., 97*, 14,249-14,257, 1992.

Vachon, P. W., O. M. Johannessen, and J. A. Johannessen, An ERS 1 synthetic aperture radar image of atmospheric lee waves, *J. Geophys. Res*., *99*, 22, 483-22,490, 1994.

Zheng, Q., X.-H. Yan, V. Klemas, C.-R. Ho, N.-J. Kuo, and Z. Wang, Coastal lee waves on ERS-1 SAR images. *J. Geophys. Res.* 103, 7979-7993, 1998.